Science of the Total Environment 646 (2019) 1615–1623

Contents lists available at ScienceDirect

Science of the Total Environment

journal homepage: www.elsevier.com/locate/scitotenv

The use of calcium carbonate-enriched clay minerals and diammonium phosphate as novel immobilization agents for mercury remediation: Spectral investigations and field applications

Jianxu Wang [a], Ying Xing [b], Yuanyan Xie [c], Yong Meng [d], Jicheng Xia [a,e], Xinbin Feng [a,*]

[a] State Key Laboratory of Environmental Geochemistry, Institute of Geochemistry, Chinese Academy of Sciences, Guiyang 550081, China
[b] School of Chemistry and Materials Science, Guizhou Normal University, Guiyang 550001, China
[c] BCEG Environmental Remediation Co., Ltd, Beijing 100015, China
[d] State Key Laboratory of Ore Deposit Geochemistry, Institute of Geochemistry, Chinese Academy of Sciences, Guiyang 550081, Guizhou, China
[e] University of Chinese Academy of Sciences, Beijing 100049, China

HIGHLIGHTS

- Calcite-enriched minerals and diammonium phosphate were used for Hg immobilization.
- Diammonium phosphate reacted with minerals to form phosphate-associated minerals.
- Mercury was immobilized with phosphate-associated minerals.
- The immobilizing agents decreased Hg bioavailability in the Hg-contaminated soils.
- The immobilizing agents inhibited crops Hg uptake.

GRAPHICAL ABSTRACT

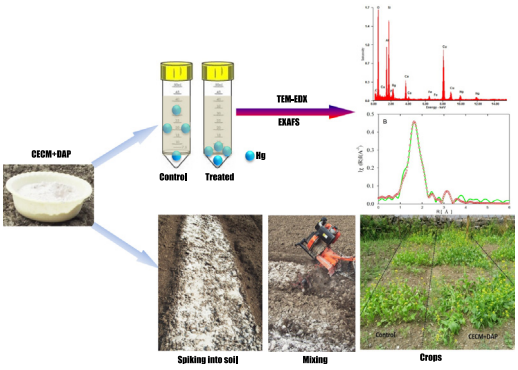

ARTICLE INFO

Article history:
Received 11 June 2018
Received in revised form 12 July 2018
Accepted 17 July 2018
Available online xxxx

Editor: Jay Gan

Keywords:
In-situ immobilization
Clay minerals
Spectral investigations
Mercury risk management

ABSTRACT

We used calcium carbonate-enriched clay minerals (CECM) and diammonium phosphate (DAP) as immobilization agents for mercury (Hg) immobilization. The effects of CECM, DAP, or both in different amounts and ratios, as well as pH and initial Hg concentrations, on Hg removal from solutions were investigated. The removal mechanism was revealed using transmission electron microscope with energy-dispersive X-ray (TEM-EDX) spectroscopy, and extended X-ray absorption fine structure spectroscopy (EXAFS). The performance of CECM and DAP under field conditions was also studied. The results showed that application of CECM and DAP at a ratio of 50:1 (w/w) removed over 90% of Hg from solutions containing 1.8 μM Hg^{2+}, which was 9- or 2.6-fold higher than solely DAP (<10%) or CECM (34%<), respectively. Mercury removal by CECM and DAP was weakly affected by pH values between 4 and 10, and their maximum Hg removal capacity was 37 mg g^{-1}. Both TEM-EDX and EXAFS results showed that the precipitate of Hg with phosphorus-associated minerals might be the primary mechanism of Hg removal by CECM and DAP. Results from the field trial showed that application of CECM and DAP decreased soil bioavailable Hg contents, but did not affect contents of organic matter bound Hg or residual Hg fractions, as compared with control and initial soils. Application of CECM and DAP resulted in dramatic reductions (40%–53%) of Hg in the edible tissues of *Brassica chinensis* and *Raphanus raphanistrum* in comparison to the non-treated control. We conclude that CECM and DAP offer a promising method for in situ remediation of Hg-contaminated farmlands in southwest of China.

* Corresponding author.
E-mail address: fengxinbin@vip.skleg.cn (X. Feng).

https://doi.org/10.1016/j.scitotenv.2018.07.225
0048-9697/

1. Introduction

Mercury (Hg) and its compounds are extremely toxic, with no known biological functions in organisms (Wang et al., 2012a). The severe health problems caused by Hg have been a major concern for many decades, and Hg is thus listed as one of the six greatest toxic threats by the Pure Earth non-governmental organization (Mills-Knapp et al., 2012). Anthropogenic sources, including Hg and gold mining, retorting and refining, the chloralkali process, coal combustion, and cement production, etc, (Wang et al., 2011a, 2012b), release 1900 to 2900 Mg of Hg into the environment annually (Driscoll et al., 2013). It is estimated that over 8 million people are at risk of exposure to Hg pollution globally (Pure Earth and Green Cross, 2016). The Hg level in non-contaminated soils is about 0.07 mg kg^{-1} (Kabata-Pendias, 2011), but it increases significantly in soils close to a Hg pollution source (Wang et al., 2011b). The current status of soil Hg pollution is problematic, especially in Asia countries such as China, Indonesia, Malaysia, where many industries and miners still used Hg and its products in Polyvinyl Chloride (PVC) production (Ren et al., 2014), artisanal and small scale gold mining activities (Gibb and O'Leary, 2014). A recent nationwide survey of soil Hg conducted by the Chinese government showed that about 1.6% of soil samples surveyed were contaminated with Hg (Zhao et al., 2015). The transfer of Hg in the soil-plant system threatens ecological safety and human health in some regions of the world (Feng et al., 2008). For example, the consumption of contaminated food products has been reported as the main pathway, by which people are exposed to Hg in areas with Hg mining in China (Zhang et al., 2010). Consequently, there is an increasing demand for remediation to mitigate the risk of Hg from soils.

Although many techniques have been developed for Hg remediation, including stabilization/solidification (S/S), vitrification, thermal desorption, nanotechnology, soil washing, electro-remediation, and biological remediation (Wang et al., 2012b), they have rarely been applied to remediating large-scale contaminated farmlands because their use may be not economically sustainable. Most Hg-contaminated farmlands remained derelict because they are economically marginal for hard redevelopment (J. Wang et al., 2018; X. Wang et al., 2018). Policymakers and engineers are increasingly aware that, when developing appropriate techniques for such farmlands, there is a need to consider comprehensively their social acceptability, affordability by the public, and fitness to the proposed use of the soils (Bardos et al., 2016). Gentle remediation options (GROs) are methods that utilize plants, fungi, and bacteria, with or without modifications, to reduce contaminants transfer into the food chain (Cundy et al., 2013). Those methods are applicable to soft-end use sites, and have lower implementation costs than physical/chemical-based remediation methods. In situ immobilization uses immobilization agents to reduce the mobility of contaminants in soils, and is considered to be a GRO due to its low cost, applicability to economically marginal land, and low risk profile (Cundy et al., 2016). The main immobilization mechanisms for Hg include adsorption onto adsorbents via electrostatic and complexation reactions (Das et al., 2007), precipitation by S^{2-} or Se^{2-} via conversion to HgS or HgSe (Zhang et al., 2012), precipitation by elemental metals (e.g., copper and zinc) via conversion to solid amalgam (He et al., 2015), and stabilization through incorporation into an insoluble matrix (e.g., $KMgPO_4 \cdot 6H_2O$ and $Mg_4Cl_2(OH)_6(H_2O)_8$) (Hagemann, 2009). Many previous studies involved testing the efficacy of FeS nanoparticles (Gong et al., 2012), tire rubber (Meng et al., 1998), phospho-gypsum (Adams et al., 2007), biochar (Shu et al., 2016), and selenium (J. Wang et al., 2018; X. Wang et al., 2018) for Hg immobilization in soils and sediments, but their applicabilities to farmlands and performance in natural environments remain unknown. There is an urgent need to develop feasible immobilization agents for contaminated farmlands. Calcium carbonate-enriched materials (e.g., mussel shells) have recently been introduced for remediating pollution of heavy metals (e.g., cadmium) due to their eco-friendly, low capital cost, easy availability, and applicability to farmlands (Peña-Rodríguez et al., 2013). The use of phosphate with those calcium carbonate-enriched materials could further improve the stabilization efficacy for toxic metals such as cadmium (Xu et al., 2017), however, their effects on Hg are poorly understood.

In this study, we used calcium carbonate-enriched clay minerals (CECM) and diammonium phosphate [$(NH_4)_2 \cdot HPO_4$] (DAP) to immobilize Hg in contaminated farmlands. The capacity of CECM and DAP to remove Hg from solutions was evaluated first, and then the removal mechanism was characterized using spectral techniques. Finally, the performance of CECM and DAP was evaluated in a natural environment. Specifically, the main objectives of this study were to (1) investigate the ability of CECM and DAP to remove Hg from solutions under various conditions, (2) characterize the mechanism of Hg removal by CECM and DAP using transmission electron microscope with energy-dispersive X-ray spectroscopy (TEM-EDX) and extended X-ray absorption fine structure (EXAFS) spectroscopy, and (3) test the efficacy of this method for treating Hg-contaminated farmlands under field conditions.

2. Materials and methods

2.1. Batch adsorption experiments

Powdered $HgCl_2$ (purity >99%), calcium carbonate-enriched clay minerals (CECM), and diammonium phosphate (DAP; agricultural grade) were purchased from a chemical company (Tianlihe Chemical Industry Co. Ltd., Guiyang, China). The chemical composition of the original CECM was characterized directly using a wavelength dispersive X-ray fluorescence spectrometer (Axios PW4400; PANalytical B.V., Netherlands). As shown in Table S1, the CECM consisted primarily of CaO, MgO, and SiO_2, with minor fractions of FeO, Al_2O_3, and K_2O. A stock solution of 2 mM $HgCl_2$ was used as the Hg pollution source for all bath experiments. Adsorption experiments were carried out using 50-mL centrifuge tubes (SuperClear™, Labcon Co. Ltd., USA), which contained negligible Hg level (<0.01 ng L^{-1}).

2.1.1. Adsorption of Hg^{2+} using CECM and/or DAP

For the separate CECM and DAP treatments, about 0.4, 1.0, 1.6, or 2.0 g of CECM or DAP was added to tubes containing 45 mL of deionized water and 1.8 μM Hg^{2+}. For the combined CECM and DAP treatments, about 0.04, 0.1, 0.13, 0.2, 0.25, 0.4, 1.6, or 2 g of DAP was added to tubes containing 45 mL of deionized water, 2 g of CECM, and 1.8 μM Hg^{2+}. Each treatment included three replicates. The tubes were shaken using a reciprocal shaker (HY-4 model; Changzhou Zhongjie Co., China) at 60 rpm for 720 min. Approximately 0.5-1 mL of solution was collected from each tube at 0, 10, 30, 60, 120, 180, and 720 min.

2.1.2. Effect of Hg^{2+} levels on Hg removal by CECM and DAP

Approximately 0.02, 0.04, 0.07, 0.11, 0.20, 0.27, 0.63, 0.99, 1.49, 2.12, 7.70, 13.41, 19.22, or 24.93 μM $HgCl_2$ was added to individual tubes containing 45 mL of deionized water, 2 g of CECM, and 0.04 g of DAP. Thus, the final Hg concentrations in the tubes were 0.4, 0.8, 1.6, 2.5, 4.5, 6.0, 14, 22, 33, 47, 171, 298, 427, or 554 μM. Tubes without Hg^{2+} treatment was also included. Each treatment was made up of three replicates. The tubes were shaken using a reciprocal shaker at 60 rpm for 720 min. Samples of the solution were taken from the tubes at 0 and 720 min.

2.1.3. Effect of pH on Hg removal by CECM and DAP

A series of tubes were prepared containing 1.8 μM Hg^{2+}, 42 mL of deionized water, 2 g of CECM, and 0.04 g of DAP. The pH of each tube was adjusted close to 4.0, 6.0, 7.0, 8.0, or 10.0 using 1 M NaOH or HCl. After pH adjustment, deionized water was added to each tube to a final volume of 45 mL. Each treatment included three replicates. The tubes were shaken using a reciprocal shaker at 60 rpm for 720 min. Samples of the solution were taken from the tubes at 0 and 720 min.

The sampled solutions were immediately passed through 0.45-μm cellulose acetate microfilters, and then acidified with Ultra-pure HCl (2%, v/v). The precipitates in the tubes containing 2 g of CECM and 0.04 g of DAP (Section 2.1.2, denoted CECM-DAP), or 2 g of CECM, 0.04 g of DAP, and 1.8 μM Hg^{2+} (Section 2.1.2, denoted CECM-DAP-Hg) were separated by centrifugation at 5000 rpm for 20 min. After separation, about 20 mL of deionized water was added to the tubes and mixed with the precipitated CECM. This suspension was shaken using a reciprocal shaker at 60 rpm for 30 min, and then the precipitates were collected by centrifugation as discussed above. The washing process was repeated three times. After washing, the precipitates were collected, freeze-dried, and stored at −18 °C for spectroscopic analysis.

2.2. Characterization of the original CECM and CECM-DAP using Fourier-transform infrared spectroscopy (FTIR), and Scanning electron microscope (SEM)-EDX spectroscopy

FTIR spectroscopic analysis: The original CECM was mixed homogeneously with KBr, and then the mixtures were pressed with a hydraulic press to form a pellet. The infrared spectra of sample was then collected under conditions ranging from 4000 to 700 cm^{-1} with peak resolution of 4 cm^{-1} using an AIM-8800 infrared microscope (Shimadzu Co., Tokyo, Japan). SEM-EDX spectroscopic analysis: Samples were coated with carbon, and their morphology and chemical compositions were characterized using a scanning electron microscope (JSM-6460LV, JEOL USA Inc., MA, America) with energy dispersive X-ray spectroscopy (EDAX, Ametek Inc, NJ, USA).

2.3. Characterization of CECM-DAP-Hg using TEM-EDX and EXAFS spectroscopy

TEM-EDX spectroscopic analysis: Freeze-dried CECM-DAP-Hg powders were dispersed with 50% ethanol, mounted in a carbon-covered copper grid, and analyzed using an analytical transmission electron microscope (Tecnai G^2 F20 S-TWIN TMP, FEI Co., America) with energy dispersive X-ray spectroscopy (EDAX, Ametek Inc, NJ, USA). EXAFS spectroscopic analysis: Freeze-dried CECM-DAP-Hg powders were pressed into a thin pellet for analysis. The reference compounds used to investigate the oxidation states and chemical structures of Hg included cinnabar (α-HgS), metacinnabar (β-HgS), mercuric oxide (HgO), mercuric chloride ($HgCl_2$), and mercuric acetate [$(CH_3COO)_2Hg$]. All Hg reference compounds were mounted on Kapton tape for Hg L_{III}-edge EXAFS spectroscopic analysis. Mercury L_{III}-edge X-ray absorption spectra were obtained at the EXAFS station (1W1B) of the Beijing Synchrotron Radiation Facility (BSRF) with 2.5 GeV electron energy, 250 mA electron current, and energy resolution (ΔE/E) of 1–3 × 10^{-4}. An energy range of −200–800 eV from the L_{III} edge of Hg (12.28 keV) was used to acquire the spectra. Data for CECM-DAP-Hg was collected in fluorescence mode using a 19-element high-purity Ge solid-state detector under ambient conditions, and data for the Hg reference compounds were obtained in transmission mode. Data normalization (background correction) along with cubic spline interpolation was performed using the IFEFFIT software package (Ravel and Newville, 2005). For data normalization, the E_0 of all Hg L_{III}-XAS spectra was set to 12,284 eV; the pre-edge range was −200 eV–45 eV and the normalization range was 150–800 eV. The background was removed using the AUTOBAK algorithm of Athena software, with the Rbkg parameter set to 1.1 and a k-weight of 2. The XANES L_{III}-edge spectral of the standards and samples were plotted with the energy ranged between 12.25 and 12.40 keV (Fig S1 in supporting information).

The Artemis program was used for EXAFS data processing. Theoretical scattering paths were calculated using FEFF, and based on the structure of model Hg compounds including HgO (Aurivillius, 1964), $Hg_3(PO_4)_2$ (Aurivillius and Nilsson, 1975), $(NH_4)_2HgCl_2(NO_3)_2$ (Peter and Gerd, 2002), and $Hg_3(AlCl_4)_2$ with partial P-for-Al substitution (Ellison et al., 1972). The shell fitting was performed on the Fourier transform real part between 1.15 and 3.5 Å using a Hanning window (dk value = 1) and optimizing over k-weights of 1, 2 and 3 (Tiberg et al., 2013). The quality of the EXAFS spectral fitting was examined by means of goodness-of-fit (R-factor), visual examination of the fitting spectral, the evaluation of the value of ΔE^0 and Debye-Waller factors (σ^2).

2.4. Field trial

A field trial was carried out at Wanshan Hg mine in southwest China. Two sites of contaminated farmlands near Hg waste piles were selected for in situ immobilization. A plot of about 12 m^2 was selected at each site, of which 6 m^2 was designated as the control, while the rest was used for CECM + DAP treatment. The application doses of CECM and DAP were 30 g and 0.5 g per kilogram of soil, respectively. Assuming that the target soil depth for remediation is 20 cm and the soil bulk density is 1.2 g cm^{-3} (Wang et al., 2011a), the total weight of the soils (6 m^2) is calculated to be 1.44 ton. Thus, 43.2 kg of CECM and 7.2 kg of DAP were added to the soils in each treated plot. After this addition, the soil and immobilization agents were homogenized using a rotary tiller (Fig. S2) at a tilling depth of 20 cm and left for one month to reach equilibrium. Seeds of pak choi (*Brassica chinensis*) and radish (*Raphanus raphanistrum*) were sown directly into each plot. Agronomic management protocols were performed manually in each field plot as required. The pak choi and radish seedlings were maintained for 50 and 156 days, respectively. During plant harvest, three individual crop samples and soil (0–20 cm depth) were collected randomly from each control and treated plot (CECM and DAP). Plant samples were washed using purified water, air-dried, and then ground to powder using an electrical grinder. Soil samples were air-dried and homogenized using an agate mortar.

2.5. Chemical analysis

The soil pH was determined using a pH meter (Hanna HI3M; Hanna Instruments INC, RI, USA) after mixing each sample with deionized water (1:2.5 w/w). Soil organic matter (OM) was measured using the method of Lu (2000). The total Hg content in the soils was determined via cold vapor atomic absorption spectrometry (CVAAS) using an F732-V Hg analyzer (Huaguang Instruments, Shanghai, China) after the digestion of sample in fresh *aqua regia* (HNO_3:HCl = 1:3, v/v) at 95 °C for 3 h. The geochemical fractions of Hg in the soils were characterized using the method of Wang et al. (2012a). The total Hg contents in plant materials were determined directly using a Lumex RA915+ mercury analyzer equipped with a Pyro 915+ pyrolysis attachment (Lumex Ltd., St. Petersburg, Russia), which has a detection limit of 0.2–5 ng g^{-1}.

2.6. Data analysis and quality assurance

The percentage of Hg removed from solutions was calculated according to the following equation (Eq. (1)):

$$Hg(\%)^{removed} = \frac{\left(Hg_{initial} - Hg_{equilibrium}\right)}{Hg_{initial}} \times 100\% \quad (1)$$

where $Hg_{removed}$ refers to the percentage of Hg removed from a solution (%); $Hg_{initial}$ represents the initial Hg concentration (mg L^{-1}) in the solutions; and $Hg_{equilibrium}$ is the Hg concentration (mg L^{-1}) in the solutions after adsorption.

The Hg removal capacity of immobilization agents was calculated as follows (Eq. (2)):

$$Q = \frac{\left(Hg_{initial} - Hg_{equilibrium}\right) \times V}{M} \quad (2)$$

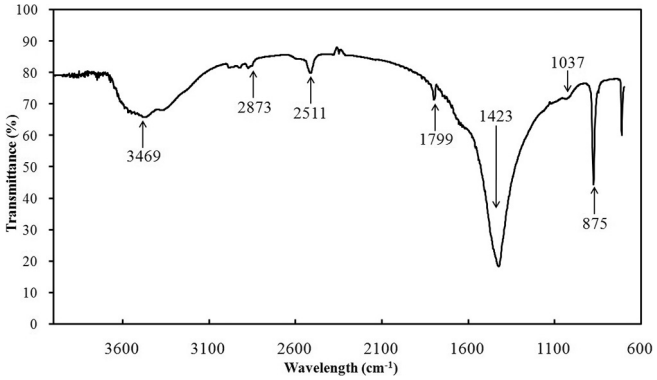

Fig. 1. Fourier transform infrared spectroscopy (FTIR) spectra of calcium carbonate-enriched clay mineral (CECM).

where Q indicates the Hg removal capacity of the immobilization agents (mg g^{-1}); $Hg_{initial}$ refers to the initial Hg concentration (mg L^{-1}) in the solutions; $Hg_{equilibrium}$ is the Hg concentration (mg L^{-1}) in the solutions after adsorption; V represents the volume of the solution (L); and M is the mass (g) of immobilization agents added.

Standard reference materials (SRM) GBW10020 and GBW (E) 070009 manufactured by the Institute of Geophysical and Geochemical Exploration, China, were utilized for plants and soils analytical QC, respectively. The average measured contents of Hg in the plant (GBW10020) and soil (GBW (E) 070009) standards were 0.13 ± 0.01 mg kg^{-1} ($n = 3$) and 2.1 ± 0.03 mg kg^{-1} ($n = 3$), respectively, which are comparable with the certified values of 0.15 ± 0.02 and 2.20 ± 0.40 mg kg^{-1}. The relative percentage difference among replicates for soil and plant samples were <11% and <8%, respectively.

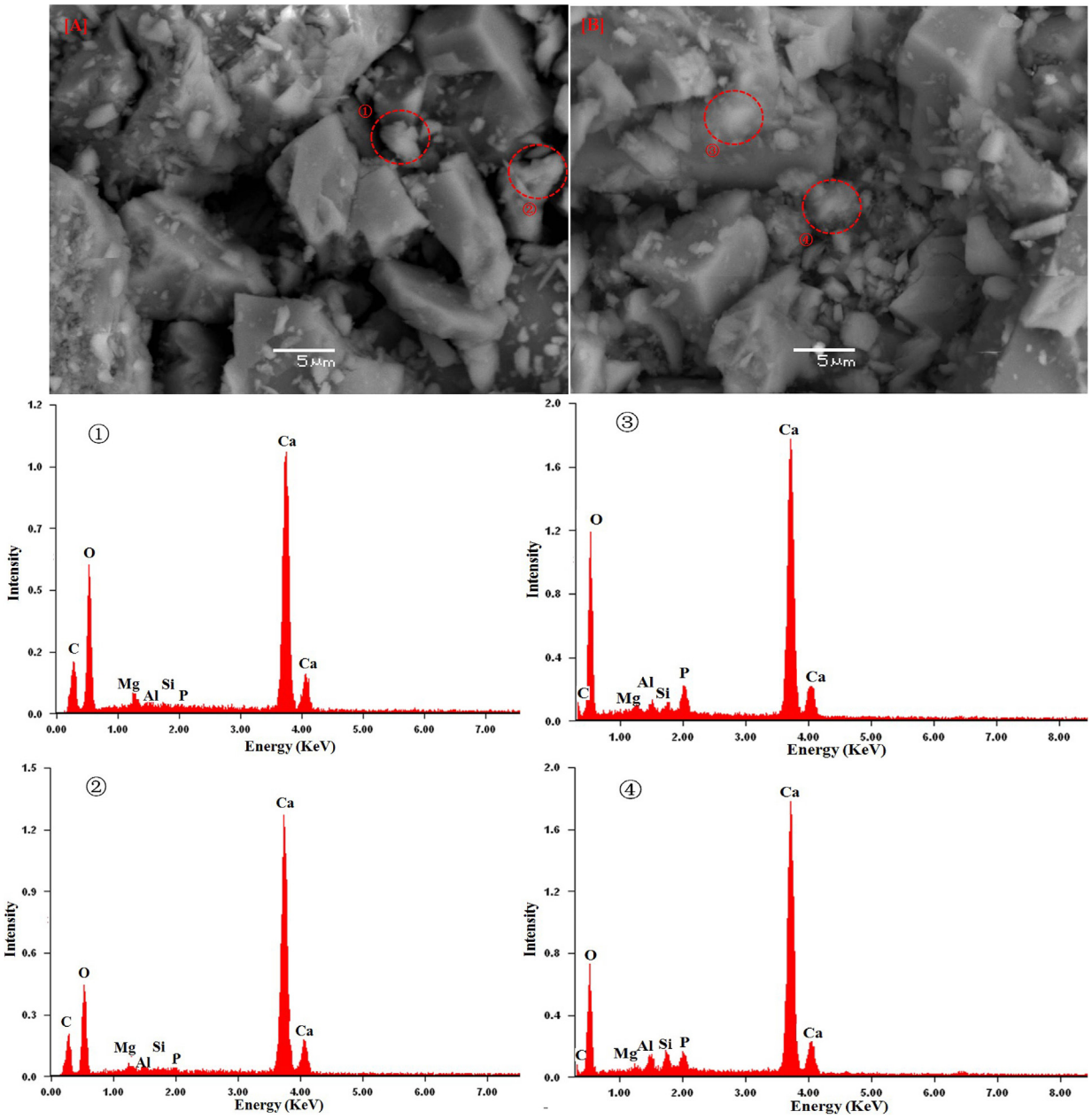

Fig. 2. Scanning electron microscopy (SEM) images and energy-dispersive X-ray (EDX) spectra obtained from four sites, showing the original calcium carbonate-enriched clay mineral (CECM) (A, ①, ②) and diammonium phosphate-modified CECM (B, ③, ④), respectively. The red circles on the SEM images show the sites where EDX analysis was conducted. (For interpretation of the references to color in this figure legend, the reader is referred to the web version of this article.)

We used SPSS software version 17.0 to perform statistical analysis. Significant differences among treatments at the $p < 0.05$ level are indicated using different lower-case letters.

3. Results and discussion

3.1. Characterization of CECM and CECM-DAP

The FTIR spectral of the original CECM is shown in Fig. 1. The presence of a broad band at 3469 cm^{-1} is probably due to the HO-H vibration of water molecules adsorbed on the silicate surface (Djomgoue and Njopwouo, 2013). Bands at 1037 cm^{-1} and 2873 cm^{-1} correspond to stretching vibration of the Si—O group (Alabarse et al., 2011) and the —CH_2 group (Tyagi et al., 2006), while 1423 cm^{-1} and 1799 cm^{-1} correspond to asymmetric stretching of the C—O bond (calcite) (George and Marcopoulos, 1995), and stretching of the C═O bond (Guo et al., 2017), respectively. Bands at 1423 cm^{-1} and 875 cm^{-1} were the characteristic of calcite (Xia et al., 2018).

The SEM images of both CECM and CECM-DAP are displayed in Fig. 2. Both the original CECM (Fig. 2-A) and CECM-DAP (Fig. 2-B) show very similar morphological properties, which were dominated by anomalous polyhedrons. However, the edges of those anomalous polyhedrons in the CECM-DAP appear flocculent (Fig. 2-A, -B). We used EDX spectroscopy to characterize the chemical compositions of the edges of those anomalous polyhedrons, and found that the main elements in both the CECM and DAP-CECM were calcium (Ca), and oxygen (O), with minor amounts of magnesium (Mg), Aluminum (Al), and Silicon (Si) (Fig. 2 ①, ②, ③, ④). However, the strong signal of phosphorus (P) was detected in the CECM-DAP. It appears that addition of DAP led to the formation of P-associated complexes in the minerals, which were associated with Ca, Mg, Al, Si, or a combination of these in the CECM-DAP.

3.2. Mercury removal by CECM and/or DAP from solutions

Fig. 3 shows the kinetics of Hg removal by CECM, DAP, and a combination of the two, which reached equilibrium at 180 min in all treatments. Application of DAP at four levels (0.9%, 2.2%, 3.5%, and 4.4%) removed <10% of Hg from the solutions (Fig. 3-A), perhaps due to the precipitation of Hg with phosphate as $Hg_3(PO_4)_2$ (Oliva et al., 2011). The CECM was more efficient for Hg removal than DAP, and its application doses of 0.9%, 2.2%, 3.5%, and 4.4% resulted in the removal of 20%–34% of Hg^{2+} from solutions. The mechanism of Hg removal by CECM might be due to the surface complexation of Hg^{2+} by hydroxyl groups (e.g., ≡SiOH) as we identified by FTIR spectroscopy (Fig. 1) (Tiffreau et al., 1995), and/or the surface precipitation of Hg^{2+} with Fe oxides (≡Fe-OHgOH) (Bonnissel-Gissinger et al., 1999). Also, the surface precipitation of Hg^{2+} with calcite-enriched minerals might occur, as observed for Cd [$(Cd,Ca)CO_3$] (Peña-Rodríguez et al., 2013). As shown in Fig. 3-B, the introduction of DAP with CECM greatly improved the removal efficacy of Hg (over 90%) in comparison to the non-DAP treatment (Fig. 3-A). The extent of this removal was enhanced with increasing mass ratio of CECM to DAP. When the ratio of CECM to DAP was 50:1, its Hg removal efficacy was similar to that of 20:1, suggesting that the reactions between Hg and CECM + DAP might reach equilibrium at this treatment level (CECM:DAP = 50:1). It seems that the higher mass ratio of CECM to DAP led to a greater removal of Hg from the solutions in our study, which might be due to the higher stability of the minerals/complexes (e.g., magnesium phosphate) produced by their reactions (Sugama and Kukacka, 1983). We further investigated the impact of pH on Hg removal by CECM and DAP (mass ratio = 50:1). As displayed in Fig. 3-C, no significant difference in Hg removal efficacy was observed when the solution's pH ranged between 4 and 10, which differed from prior studies on clay minerals showing that Hg adsorption was affected significantly by pH. For example, the maximum adsorption of Hg by bentonite occurred at acidic pH condition (pH

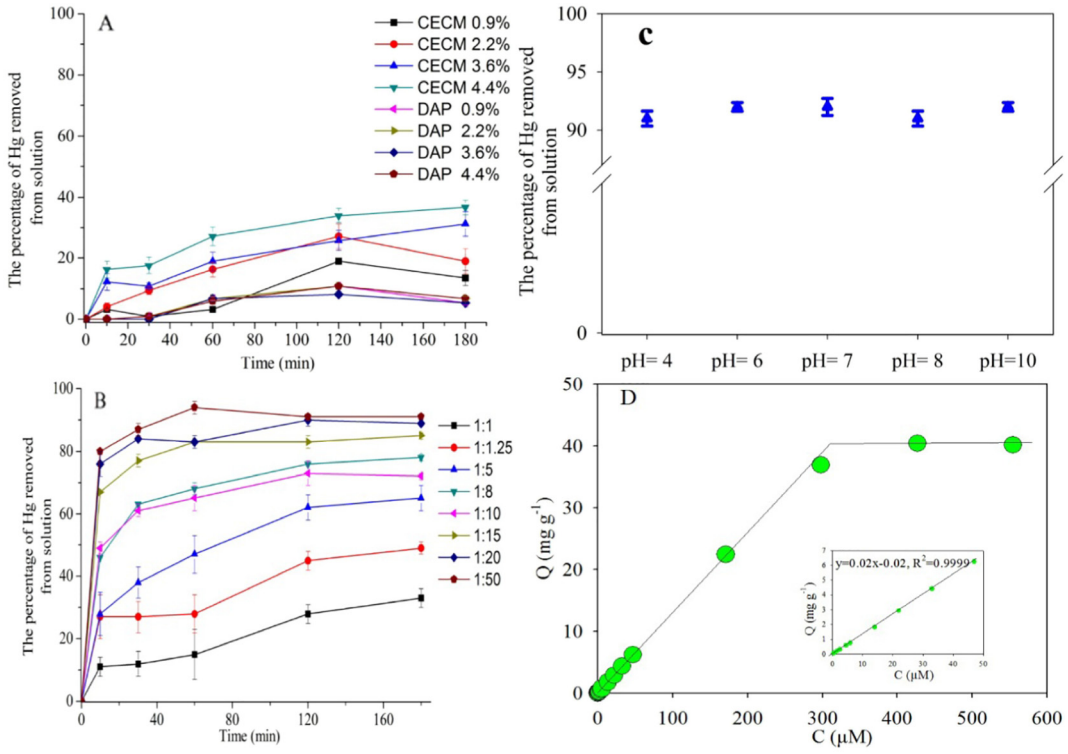

Fig. 3. The kinetics of Hg removal by calcium carbonate-enriched clay minerals (CECM), diammonium phosphate (DAP), and a combination of CECM and DAP at different treatment levels in solutions containing 1.8 μM Hg^{2+} (A: Hg removal by CECM or DAP; B: Hg removal by CECM and DAP). The impact of pH on Hg removal by CECM+DAP (50:1, w/w) from the solutions (C), and the impact of initial concentrations of Hg in the solutions on Hg removal by CECM and DAP (50:1, w/w) (D). Error bar indicates the standard deviation of three replicates; The legend 1:1, 1:1.25, 1:5, 1:8, 1:10, 1:15, 1:20, and 1:50 means the ratio of DAP to CECM (w/w) (B); Q means the Hg removal capacity of the immobilization agent (mg g^{-1}) (D).

= 3–3.5) (Viraraghavan and Kapoor, 1994), while by laterite appeared at alkaline condition (pH = 8) (Yu et al., 2008). The pH affects Hg removal by clay minerals mainly through changing the Hg speciation in the solution. The adsorption of Hg by hydroxyl groups favored acidic environment because of the dominance of Hg^{2+} and $HgOH^{+}$ in the solutions (Viraraghavan and Kapoor, 1994). The less impact of pH (4–10) on Hg removal by CECM and DAP indicates that this Hg immobilization process is relatively resistant to the change of the Hg speciation in the solutions, perhaps through a mechanism of co-precipitation. The maximum removal capacity (Q) of 37 mg g^{-1} was obtained with a solution containing 2 g of CECM and 0.04 g of DAP. The Hg removal capacity of CECM and DAP was similar to that of other naturally-produced sorbents, but lower than the synthesized- and chemically-modified sorbents reported by prior studies, as shown in Table S2. The characterization of isotherm for Hg^{2+} can be described using a linear isotherm over the Hg concentration range of 0.4 to 298 μM in the solutions (Fig. 3-D). When Hg concentration exceeds about 298 μM, its removal reached equilibrium. The linear isotherm model for Hg^{2+} removal by CECM and DAP differ from previous studies where the Langmuir isotherm and the power function kinetic model was used for Hg^{2+} removal by biochar (O'Connor et al., 2018) and water treatment residual nanoparticles (Elkhatib et al., 2017), respectively. The presence of linear isotherm indicates the constant removal of ions by the minerals, perhaps due to the change of internal structure of adsorbents makes more available sites for reaction. Giles et al. (1974) illustrated that the changed site in those adsorbents could be in a structure similar with "micropore", and the process of contaminants penetration into the "micropore" thus proceeds steadily since the "micropore" remains constant in number until they are occupied. We characterized the chemical speciation of Hg in CECM-DAP-Hg by methods of TEM-EDX and EXAFS spectroscopy to reveal the mechanism of Hg immobilization by CECM and DAP.

3.3. Chemical speciation of Hg in CECM-DAP-Hg

As shown in Fig. 4, the edge of the mineral particle (thick and dark area) was surrounded by filamentous or floccus-like deposits, comparable with SEM images (Fig. 2). Those filamentous or floccus-like deposits might be the products from the reactions of CECM and DAP, which mainly consisted of Ca-, Mg-, Al-, Si-, P-, and Fe-containing minerals as evidenced by EDX spectroscopy. We did not detect any Hg signal in the mineral particles surveyed (thick and black area), but detected that in those filamentous or floccus-like deposits (Fig. 4-A, -B). It thus appears that Hg might associate with Ca, Mg, Al, Si, and Fe in the studied minerals. However, the reactions between DAP and Si or Fe oxides were rarely reported and appeared to be difficult to proceed under natural condition (Taylor et al., 1965), while that and $CaCO_3$ or Mg oxides had been documented (da Silva et al., 2016; Kirinovic et al., 2017). The $(NH_4)_2HPO_4$ reacted with $CaCO_3$ and Mg oxides to produce calcium

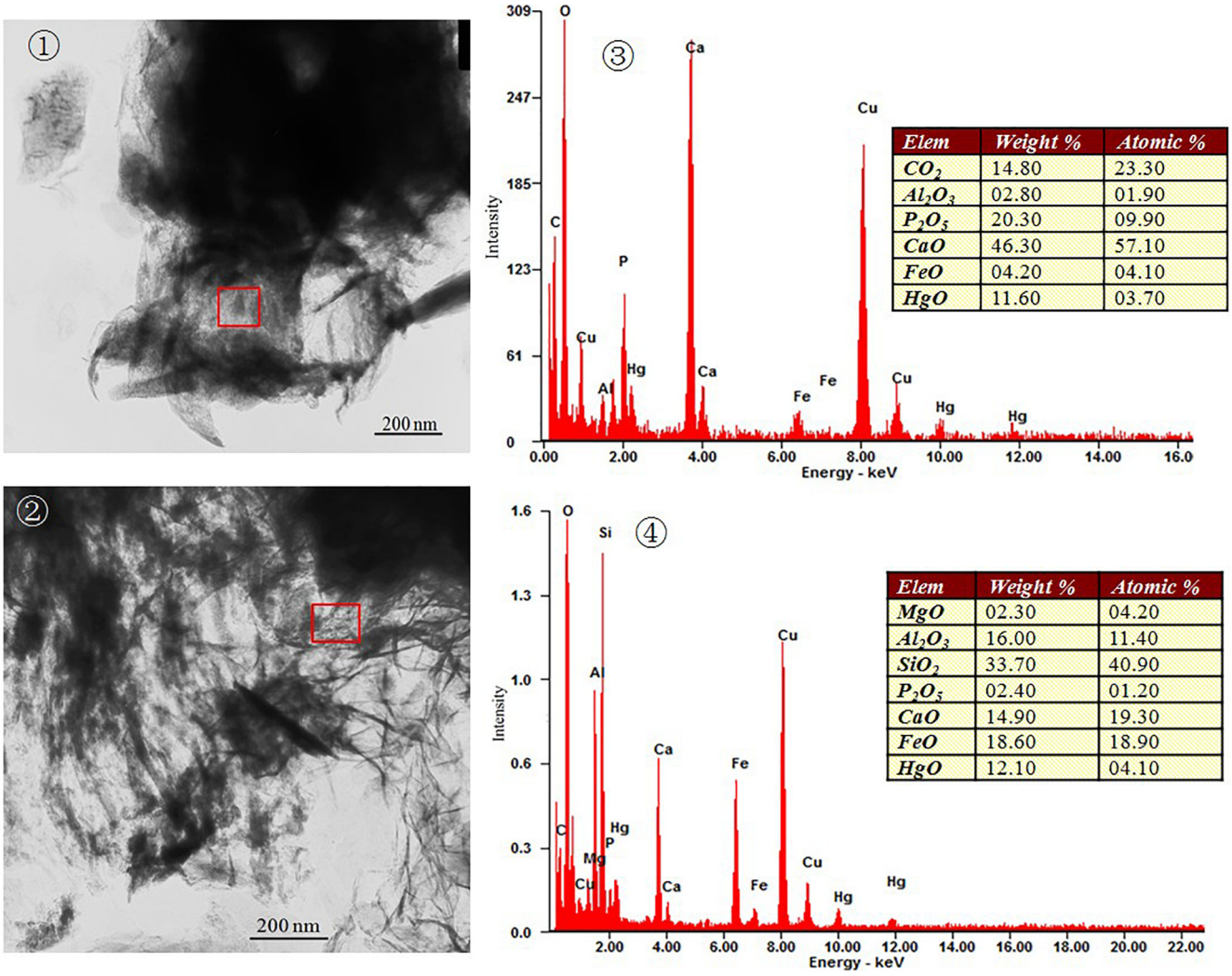

Elem	Weight %	Atomic %
CO_2	14.80	23.30
Al_2O_3	02.80	01.90
P_2O_5	20.30	09.90
CaO	46.30	57.10
FeO	04.20	04.10
HgO	11.60	03.70

Elem	Weight %	Atomic %
MgO	02.30	04.20
Al_2O_3	16.00	11.40
SiO_2	33.70	40.90
P_2O_5	02.40	01.20
CaO	14.90	19.30
FeO	18.60	18.90
HgO	12.10	04.10

Fig. 4. Transmission electron microscopy images (① and ②) and energy-dispersive X-ray (EDX) spectra (③ and ④) of CECM-DAP-Hg. The red squares on the TEM images show the sites where EDX analysis was conducted. Copper signals derive from the copper grid. (For interpretation of the references to color in this figure legend, the reader is referred to the web version of this article.)

phosphate gel (L. Wang et al., 2012) and magnesium phosphate (Buj et al., 2010) respectively, which have been documented to be able to immobilize Cr^{3+}, Cu^{2+}, Pb^{2+}, Zn^{2+} and Cd^{2+} via adsorption, surface complexation, bulk substitution and the precipitation of metal-bearing phases (Rouff, 2012; Rouff et al., 2016; Cho et al., 2014; Lyczko et al., 2014). Those reactions might have happened in our study, and contributed to Hg removal. We further studied the Hg coordination environment in the CECM-DAP-Hg using EXAFS spectroscopy to demonstrate which elements coordinated with Hg.

The Hg L_{III}-edge XANES spectra of Hg standards and CECM-DAP-Hg is shown in Fig. S1. A weak adsorption peak at 12.289 keV was found in the near-edge region of Hg L_{III}-edge spectra for HgO and $HgCl_2$, which could be due to the 2p to $5d_z^2$ electron transition (Gibson et al., 2011). Also, the Hg L_{III}-edge spectra for CECM-DAP-Hg was characterized by a small peak at 12.289 keV, suggesting that Hg in CECM-DAP-Hg presents in a similar coordination environment as $HgCl_2$ or HgO, in which Hg coordinated linearly with two oxygen or chloride atoms (Manceau et al., 2015). Further structural information on CECM-DAP-Hg was revealed by EXAFS analysis. The k^2-weighted EXAFS spectra, and corresponding Fourier-transform magnitude for the CECM-DAP-Hg is shown in Fig. 5. The calculated values of R-factor, ΔE_0 and Debye-Waller value (σ^2) were 0.006, 3.16, and 0.003–0.02 (Table 1), respectively, comparable with previously reported values (Kim et al., 2004). Spectral for Hg of CECM-DAP-Hg was modeled with the first scattering path of HgO (Hg-O). Thereafter, we compared the fitting results from different models for optimal fits, and found that the fit was improved noticeably when we used the first three paths from theoretical models of HgO [First path, Hg-O], $Hg_3(AlCl_4)_2$ with partial P-for-Al substitution [second path: Hg-P], $Hg_3(PO_4)_2$ [third path: Hg-P], and $(NH_4)_2HgCl_2(NO_3)_2$ [fourth path: Hg-N]. Estimated bond length of Hg-O, Hg-P, Hg-P, and Hg-N was 2.01 Å, 2.34 Å, 3.07 Å and 3.62 Å respectively. The coordination numbers are 2 for Hg for all the shells, indicative of a linear -N-P-P-O-Hg-O-P-P-N- configuration. The Hg-O distance (2.01 Å) derived from EXAFS spectral fit of CECM-DAP-Hg was comparable with that of Hg(II) sorption on mineral surfaces of goethite, γ-alumina, and bayerite where the Hg-O distances were reported as 1.99–2.07 Å (Kim et al., 2004; Serrano et al., 2012). The presence of two Hg-P bonds at the second and third shells is consistent with the observation of the close association between P and Hg in the CECM-DAP-Hg as shown by our TEM-EDX results. Also, considering the low molar ratio of Hg/P of the CECM-DAP-Hg of 0.01, Hg atoms could be surrounded by P atoms. We observed Hg-N bond at the fourth shell, demonstrating the involvement of NH_4^+ in the reaction.

In summary, our TEM-EDX and EXAFS results showed that the reaction of CECM and DAP led to the formation of filamentous and/or floccus-like deposits, in which Hg might be immobilized by precipitating with P-associated minerals (e.g., calcium phosphate gel, magnesium phosphate) (Lyczko et al., 2014; L. Wang et al., 2012) as $-HgO_2P_2P_2N_2-$ configuration.

3.4. Field trial

As shown in Fig. S2, we conducted field trials to investigate the potential of using CECM and DAP for treating contaminated farmlands. Two experimental plots had soil Hg contents of 107 and 58 mg kg^{-1}, which are 71- and 39-fold, respectively, above the maximum allowable Hg content determined by the Chinese government for farmland (CNEPA, 1995). The pH of these soil samples was neutral to slightly alkaline, and organic matter content was 44–46 g kg^{-1} (Table S3). These plots were chosen because they were still under cultivation.

The geochemical fractions of Hg in the soils were characterized before and after the experiment (Fig. S3). No significant fractionation of Hg was observed between the control and initial soils, suggesting that growing crops had a weaker effect on Hg geochemical fractionation in our soils (Wang et al., 2017). The application of both CECM and DAP significantly decreased the bioavailable Hg content (sum of soluble and exchangeable, and specifically sorbed Hg) by 43%–54% compared to both initial and untreated (control) soils in two experimental farmlands. This finding is compatible with our adsorption experiment, wherein both CECM and DAP caused a significant reduction in the Hg concentration of the solution (Fig. 3). The mechanism of this Hg reduction in the soils might be the one that we proposed in Section 3.3. In the plot where pak choi was grown, the content of Fe/Mn oxides in the treated soils also decreased noticeably, by 62%–66%, compared with the levels in both the initial and control soils. However, the differences in the organic-bound and residual Hg fractions among the initial, control, and treated soils were not significant in two experimental plots. The application of CECM and DAP significantly increased the fresh biomass of pak choi roots and shoots compared with that in the control (Fig. S2-D; Table 2), whereas this treatment did not notably affect the biomass of radish. The increase of biomass in pak choi is probably due to enhanced fertility and improved soil structure by DAP and CECM (Bronick and Lal, 2005). Therefore, both CECM and DAP may be used to treat contaminated farmlands at Wanshan Hg mine without reducing the biomass yield of the crops.

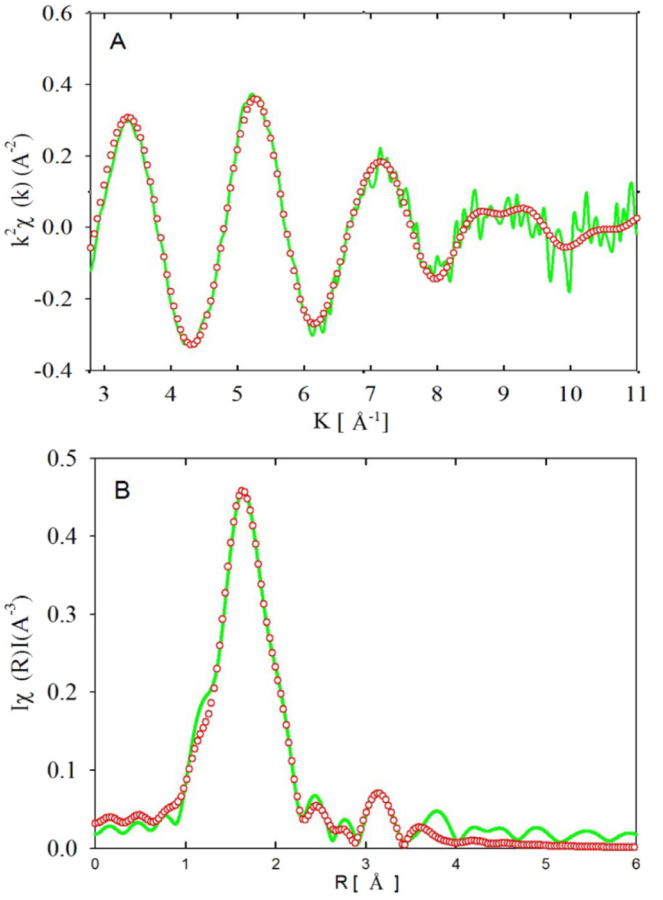

Fig. 5. The k^2-weighted EXAFS spectra (A), and corresponding Fourier-transform magnitude (B) for the CECM-DAP-Hg. Green solid lines are data and red dashed lines are nonlinear least-squares fits. (For interpretation of the references to color in this figure legend, the reader is referred to the web version of this article.)

Table 1
Simulated Hg L_{III}-edge EXAFS parameters for CECM-DAP-Hg.

Sample	K range (Å)	Path	CN	ΔE_0	R (Å)	σ^2 ($Å^2$)	R-factor
CECM-DAP-Hg	2.8–10.8	Hg-O	2[a]	3.19	2.01	0.007	0.006
	2.8–10.8	Hg-P	2[a]	3.19	2.34	0.009	0.006
	2.8–10.8	Hg-P	2[a]	3.19	3.07	0.003	0.006
	2.8–10.8	Hg-N	2[a]	3.19	3.62	0.02	0.006

[a] Means the coordination numbers are derived from the model compounds.

Table 2
Pakchoi's and Radish's fresh biomass yield [g] and Hg contents [mg Hg per kg of fresh biomass]. Mean ± sd ($n = 3$).

Treatments		Pakchoi root	Pakchoi shoot	Radish root
Control	Biomass yield [g]	0.4 ± 0.07 a	3.5 ± 0.2 a	73.8 ± 5.7 a
	Hg content [mg kg^{-1}]	0.08 ± 0.04 a	0.4 ± 0.006 a	0.015 ± 0.005 a
CECM + DAP	Biomass yield [g]	1.2 ± 0.2 b	8.8 ± 1.8 b	83.1 ± 10.4 a
	Hg content [mg kg^{-1}]	0.04 ± 0.01 b	0.24 ± 0.05 b	0.007 ± 0.002 b

The different lower case letters in each column means the difference in biomass yield or Hg content between control and CECM + DAP treatment is significant at $p < 0.05$. According to the Chinese environmental quality for food products (GB 2762–2012), the maximum allowable Hg content in the edible section of vegetables is 10 ng g^{-1} [mg Hg per kg of fresh biomass].

The contents of Hg in the shoots of pak choi (0.4 mg kg^{-1}) and roots of radish (0.015 mg kg^{-1}) (edible sections) grown in the untreated soils were 40- and 1.5-fold higher than the maximum allowable Hg content in the edible section of vegetables (0.01 mg kg^{-1}; fresh weight) based on food quality standards set by the Chinese government (CNEPA, 2012). The application of CECM + DAP dramatically decreased the Hg content in the roots and shoots of pak choi and the roots of radish by 50%, 40%, and 53%, respectively, compared with the level in the corresponding controls (Table 2). It should be noted that the Hg contents in the roots of radish in the treated soils were lower than the Chinese standard (CNEPA, 2012). These results might be explained by the reduction of the bioavailable Hg pool in the soils by CECM and DAP.

Our work showed promising results in the form of a significant reduction of the Hg content in the edible sections of two crops after CECM and DAP treatment, in particular lowering the content of Hg in radish roots below the Chinese food quality standard. It should be noted that a certain proportion of Hg in the shoots of pak choi might be sourced from the atmosphere (Manceau et al., 2018), as the recorded atmospheric Hg^0 concentrations of 17–2100 ng m^{-3} at Wanshan Hg mine (Dai et al., 2012) could lead to Hg accumulation by leaves. Thus, despite decreased bioavailable Hg in the soil, Hg might be adsorbed from the atmosphere into the shoot. In this context, CECM and DAP may be used to decrease the bioavailable Hg content of contaminated soil, and prevent its transfer into crops. Meanwhile, the long-term performance of our immobilizing agents in Wanshan soils will be revealed in our future studies.

4. Conclusions

The application of CECM and DAP efficiently removed Hg^{2+} from solutions (>90%) after 180 min, and the optimum ratio of CECM to DAP was 50:1 (w/w). Mercury removal was minimally affected by CECM and DAP when the pH values ranged between 4 and 10 in our solutions. The maximum removal rate of Hg by CECM and DAP was 37 mg g^{-1}. The removal of Hg by CECM and DAP may be through a mechanism of a precipitation of Hg by P-associated minerals, as evidenced by the TEM-EDX, and EXAFS results. The application of CECM and DAP significantly decreased the bioavailable Hg content compared with those in the initial and control soils, but did not affect the geochemical forms of Hg associated with the organic matter and residual fractions. The application of CECM and DAP significantly increased the biomass yield of pak choi compared with that of the control, but did not affect that of radish. In addition, CECM and DAP treatments resulted in dramatic reduction (40%–53%) of Hg content in the two crops, particularly for the content of Hg in the radish roots to below the Chinese food quality standard. The results of this study suggest that CECM and DAP may be used to remediate contaminated farmlands in the Hg mining region in southwest China.

Acknowledgements

This work was supported by the Natural Science Foundation of China [41573082, 41703116, 41303068]; and the Opening Fund of the State Key Laboratory of Environmental Geochemistry [SKLEG2015903, SKLEG2017907, SKLEG2017912]. Many thanks go to the 1W1B beam station at Beijing Synchrotron Radiation Facility for supporting the Hg L_{III}-edge EXAFS analysis.

Appendix A. Supplementary data

Supplementary data to this article can be found online at https://doi.org/10.1016/j.scitotenv.2018.07.225.

References

Adams, E., García-Sánchez, A., Santos, F., Velázquez, E., Adams-Meléndez, M., 2007. Immobilization of Mercury in Soils of Venezuela Using Phospho-gypsum and Sulphate-reducing Bacteria. Springer Netherlands, Dordrecht, pp. 333–336.
Alabarse, F.G., Conceição, R.V., Balzaretti, N.M., Schenato, F., Xavier, A.M., 2011. In-situ FTIR analyses of bentonite under high-pressure. Appl. Clay Sci. 51, 202–208.
Aurivillius, K., 1964. Least-squares Refinement of Crystal Structures of Orthorhombic HgO + of $Hg^{202}NAI$, *Acta Chem Scand.***18**. 1305-1306.
Aurivillius, K., Nilsson, B.A., 1975. The crystal structure of mercury (II) phosphate, $Hg_3(PO_4)_2$. Z. Kristallogr. Cryst. Mater. 141, 1–10.
Bardos, R.P., Cundy, A.B., Smith, J.W.N., Harries, N., 2016. Sustainable remediation. J. Environ. Manag. 184: 1–3.
Bonnissel-Gissinger, P., Alnot, M., Lickes, J.-P., Ehrhardt, J.-J., Behra, P., 1999. Modeling the adsorption of mercury(II) on (hydr)oxides II: α-FeOOH (goethite) and amorphous silica. J. Colloid Interface Sci. 215, 313–322.
Bronick, C.J., Lal, R., 2005. Soil structure and management: a review. Geoderma 124, 3–22.
Buj, I., Torras, J., Rovira, M., de Pablo, J., 2010. Leaching behaviour of magnesium phosphate cements containing high quantities of heavy metals. J. Hazard. Mater. 175, 789–794.
Cho, J.H., Eom, Y., Lee, T.G., 2014. Stabilization/solidification of mercury-contaminated waste ash using calcium sodium phosphate (CNP) and magnesium potassium phosphate (MKP) processes. J. Hazard. Mater. 278, 474–482.
CNEPA (Chinese National Environment Protect Agency), 1995. Environmental Quality Standard for Soils (in Chinese); GB15618-1995. pp. 1–6.
CNEPA (Chinese National Environment Protect Agency), 2012. Environmental Quality Standard for Food Products (in Chinese); GB 2762–2012. pp. 1–17.
Cundy, A.B., Bardos, R.P., Church, A., Puschenreiter, M., Friesl-Hanl, W., Müller, I., et al., 2013. Developing principles of sustainability and stakeholder engagement for "gentle" remediation approaches: the European context. J. Environ. Manag. 129, 283–291.
Cundy, A., Bardos, R., Puschenreiter, M., Mench, M., Bert, V., Friesl-Hanl, W., et al., 2016. Brownfields to green fields: realising wider benefits from practical contaminant phytomanagement strategies. J. Environ. Manag. 184, 67–77.
da Silva, N.M.P., Espitalier, F., Nzihou, A., 2016. Precipitation process of calcium phosphate from calcium carbonate suspension. KONA Powder Part. J. 33, 219–227.
Dai, Z., Feng, X., Sommar, J., Li, P., Fu, X., 2012. Spatial distribution of mercury deposition fluxes in Wanshan Hg mining area, Guizhou province, China. Atmos. Chem. Phys. 12, 6207–6218.
Das, S.K., Das, A.R., Guha, A.K., 2007. A study on the adsorption mechanism of mercury on aspergillus versicolor biomass. Environ. Sci. Technol. 41, 8281–8287.
Djomgoue, P., Njopwouo, D., 2013. FT-IR spectroscopy applied for surface clays characterization. J. Surf. Eng. Mater. Adv. Technol. 3, 275–282.
Driscoll, C.T., Mason, R.P., Chan, H.M., Jacob, D.J., Pirrone, N., 2013. Mercury as a global pollutant: sources, pathways, and effects. Environ. Sci. Technol. 47, 4967–4983.
Elkhatib, E., Moharem, M., Mahdy, A., Mesalem, M., 2017. Sorption, release and forms of mercury in contaminated soils stabilized with water treatment residual nanoparticles. Land Degrad. Dev. 28, 752–761.
Ellison, R.D., Levy, H.A., Fung, K.W., 1972. Crystal and molecular structure of trimercury chloroaluminate, $Hg_3(AlCl_4)_2$. Inorg. Chem. 11, 833–836.
Feng, X., Li, P., Qiu, G., Wang, S., Li, G., Shang, L., et al., 2008. Human exposure to methylmercury through rice intake in mercury mining areas, Guizhou Province, China. Environ. Sci. Technol. 42, 326–332.
George, E., Marcopoulos, I., 1995. Origin of the bentonite deposits of eastern Milos, Aegean, Greece: geological, mineralogical and geochemical evidence. Clay Clay Miner. 43, 63–77.
Gibb, H., O'Leary, K.G., 2014. Mercury exposure and health impacts among individuals in the artisanal and small-scale gold mining community: a comprehensive review. Environ. Health Perspect. 122, 667–672.
Gibson, B.D., Ptacek, C.J., Lindsay, M.B.J., Blowes, D.W., 2011. Examining mechanisms of groundwater Hg(II) treatment by reactive materials: an EXAFS study. Environ. Sci. Technol. 45, 10415–10421.
Giles, C.H., Smith, D., Huitson, A., 1974. A general treatment and classification of the solute adsorption isotherm. I. Theoretical. J. Colloid Interface Sci. 47, 755–765.
Gong, Y., Liu, C., Xiong, Z., Kaback, D., Zhao, D., 2012. Immobilization of mercury in field soil and sediment using carboxymethyl cellulose stabilized iron sulfide nanoparticles. Nanotechnology 23, 294007.

Guo, Z., Li, J., Guo, Z., Guo, Q., Zhu, B., 2017. Phosphorus removal from aqueous solution in parent and aluminum-modified eggshells: thermodynamics and kinetics, adsorption mechanism, and diffusion process. Environ. Sci. Pollut. Res. 24, 14525–14536.
Hagemann, S., 2009. Technologies for the stabilization of elemental mercury and mercury-containing wastes. Gesellschaft für Anlagen-und Reaktorsicherheit (GRS).
He, F., Gao, J., Pierce, E., Strong, P.J., Wang, H., Liang, L., 2015. In situ remediation technologies for mercury-contaminated soil. Environ. Sci. Pollut. Res. 22, 8124–8147.
Kabata-Pendias, A., 2011. Trace Elements in Soils and Plants. fourth ed. CRC Press, Boca Raton, USA.
Kim, C.S., Rytuba, J.J., Brown Jr., G.E., 2004. EXAFS study of mercury(II) sorption to Fe- and Al-(hydr)oxides: II. Effects of chloride and sulfate. J. Colloid Interface Sci. 270, 9–20.
Kirinovic, E., Leichtfuss, A.R., Navizaga, C., Zhang, H., Schuttlefield Christus, J.D., Baltrusaitis, J., 2017. Spectroscopic and microscopic identification of the reaction products and intermediates during the struvite ($MgNH_4PO_4 \cdot 6H_2O$) formation from magnesium oxide (MgO) and magnesium carbonate ($MgCO_3$) microparticles. ACS Sustain. Chem. Eng. 5, 1567–1577.
Lu, R., 2000. Chemical Analysis Method of Agricultural Soil. China Agricultural Science Press, Beijing (In Chinese).
Lyczko, N., Nzihou, A., Sharrok, P., 2014. Calcium phosphate sorbent for environmental application. Procedia Eng. 83, 423–431.
Manceau, A., Lemouchi, C., Enescu, M., Gaillot, A.C., Lanson, M., Magnin, V., et al., 2015. Formation of mercury sulfide from Hg(II)-thiolate complexes in natural organic matter. Environ. Sci. Technol. 49, 9787–9796.
Manceau, A., Wang, J., Rovezzi, M., Glatzel, P., Feng, X., 2018. Biogenesis of mercury–sulfur nanoparticles in plant leaves from atmospheric gaseous mercury. Environ. Sci. Technol. 52, 3935–3948.
Meng, X., Hua, Z., Dermatas, D., Wang, W., Hsiu Yu, K., 1998. Immobilization of mercury (II) in contaminated soil with used tire rubber. J. Hazard. Mater. 57, 231–241.
Mills-Knapp, S., Traore, K., Ericson, B., Keith, J., Hanrahan, D., Caravanos, J., 2012. The World's Worst Pollution Problems: Assessing Health Risks at Hazardous Waste Sites. Blacksmith Institute, New York.
O'Connor, D., Peng, T., Li, G., Wang, S., Duan, L., Mulder, J., et al., 2018. Sulfur-modified rice husk biochar: a green method for the remediation of mercury contaminated soil. Sci. Total Environ. 621, 819–826.
Oliva, J., De Pablo, J., Cortina, J.-L., Cama, J., Ayora, C., 2011. Removal of cadmium, copper, nickel, cobalt and mercury from water by Apatite II™: column experiments. J. Hazard. Mater. 194, 312–323.
Peña-Rodríguez, S., Bermúdez-Couso, A., Nóvoa-Muñoz, J.C., Arias-Estévez, M., Fernández-Sanjurjo, M.J., Álvarez-Rodríguez, E., et al., 2013. Mercury removal using ground and calcined mussel shell. J. Environ. Sci. 25, 2476–2486.
Peter, N., Gerd, M., 2002. Ammonium mercury(II) dichloride nitrate, $(NH_4)_2HgCl_2(NO_3)_2$. Acta Cryst. E 58, i68–i69.
Pure Earth, Green Cross, 2016. The World's Worst Pollution Problems: Assessing Health Risks at Hazardous Waste Sites. vol. 23. Blacksmith Institute, New York, Zürich.
Ravel, B., Newville, M., 2005. ATHENA, ARTEMIS, HEPHAESTUS: data analysis for X-ray absorption spectroscopy using IFEFFIT. J. Synchrotron Radiat. 12, 537–541.
Ren, W., Duan, L., Zhu, Z., Du, W., An, Z., Xu, L., 2014. Mercury transformation and distribution across a polyvinyl chloride (PVC) production line in China. Environ. Sci. Technol. 48, 2321–2327.
Rouff, A.A., 2012. Sorption of chromium with struvite during phosphorus recovery. Environ. Sci. Technol. 46, 12493–12501.
Rouff, A.A., Ramlogan, M.V., Rabinovich, A., 2016. Synergistic removal of zinc and copper in greenhouse waste effluent by struvite. ACS Sustain. Chem. Eng. 4, 1319–1327.
Serrano, S., Vlassopoulos, D., Bessinger, B., O'Day, P.A., 2012. Immobilization of hg(II) by coprecipitation in sulfate-cement systems. Environ. Sci. Technol. 46, 6767–6775.
Shu, R., Wang, Y., Zhong, H., 2016. Biochar amendment reduced methylmercury accumulation in rice plants. J. Hazard. Mater. 313, 1–8.
Sugama, T., Kukacka, L.E., 1983. Magnesium monophosphate cements derived from diammonium phosphate solutions. Cem. Concr. Res. 13, 407–416.
Taylor, A.W., Gurney, E.L., Frazier, A.W., 1965. Precipitation of phosphate from ammonium phosphate solutions by iron oxide and aluminum hydroxide1. Soil Sci. Soc. Am. J. 29, 317–320.
Tiberg, C., Sjöstedt, C., Persson, I., Gustafsson, J.P., 2013. Phosphate effects on copper (II) and lead (II) sorption to ferrihydrite. Geochim. Cosmochim. Acta 120, 140–157.
Tiffreau, C., Lützenkirchen, J., Behra, P., 1995. Modeling the adsorption of mercury(II) on (hydr)oxides: I. Amorphous iron oxide and α-quartz. J. Colloid Interface Sci. 172, 82–93.
Tyagi, B., Chudasama, C.D., Jasra, R.V., 2006. Determination of structural modification in acid activated montmorillonite clay by FT-IR spectroscopy. Spectrochim. Acta A Mol. Biomol. Spectrosc. 64, 273–278.
Viraraghavan, T., Kapoor, A., 1994. Adsorption of mercury from wastewater by bentonite. Appl. Clay Sci. 9, 31–49.
Wang, J.X., Feng, X.B., Anderson, C.W.N., Qiu, G.L., Ping, L., Bao, Z.D., 2011a. Ammonium thiosulphate enhanced phytoextraction from mercury contaminated soil - results from a greenhouse study. J. Hazard. Mater. 186, 119–127.
Wang, J.X., Feng, X.B., Anderson, C.W.N., Zhu, W., Yin, R.S., Wang, H., 2011b. Mercury distribution in the soil-plant-air system at the Wanshan mercury mining district in Guizhou, Southwest China. Environ. Toxicol. Chem. 30, 2725–2731.
Wang, L., Ruiz-Agudo, E., Putnis, C.V., Menneken, M., Putnis, A., 2012. Kinetics of calcium phosphate nucleation and growth on calcite: implications for predicting the fate of dissolved phosphate species in alkaline soils. Environ. Sci. Technol. 46, 834–842.
Wang, J.X., Feng, X.B., Anderson, C.W.N., Wang, H., Zheng, L.R., Hu, T.D., 2012a. Implications of mercury speciation in thiosulfate treated plants. Environ. Sci. Technol. 46, 5361–5368.
Wang, J.X., Feng, X.B., Anderson, C.W.N., Xing, Y., Shang, L.H., 2012b. Remediation of mercury contaminated sites - a review. J. Hazard. Mater. 221, 1–18.
Wang, J.X., Xia, J.C., Feng, X.B., 2017. Screening of chelating ligands to enhance mercury accumulation from historically mercury-contaminated soils for phytoextraction. J. Environ. Manag. 186, 233–239.
Wang, J., Xing, Y., Li, P., Xia, J., Liu, T., Feng, X., 2018. Chemically-assisted phytoextraction from metal(loid)s-polluted soils at a typical carlin-type gold mining area in Southwest China. J. Clean. Prod. 189, 612–619.
Wang, X., Song, W., Qian, H., Zhang, D., Pan, X., Gadd, G.M., 2018. Stabilizing interaction of exopolymers with nano-Se and impact on mercury immobilization in soil and groundwater. Environ. Sci. Nano 5, 456–466.
Xia, X., Chen, J., Shen, J., Huang, D., Duan, P., Zou, G., 2018. Synthesis of hollow structural hydroxyapatite with different morphologies using calcium carbonate as hard template. Adv. Powder Technol. 29, 1562–1570.
Xu, Y., Liang, X., Xu, Y., Qin, X., Huang, Q., Wang, L., 2017. Remediation of heavy metal-polluted agricultural soils using clay minerals: a review. Pedosphere 27, 193–204.
Yu, X., Zhu, L., Guo, B., He, S., 2008. Adsorption of mercury on laterite from Guizhou Province, China. J. Environ. Sci. 20, 1328–1334.
Zhang, H., Feng, X.B., Larssen, T., Qiu, G.L., Vogt, R.D., 2010. In inland China, rice, rather than fish, is the major pathway for methylmercury exposure. Environ. Health Perspect. 118, 1183–1188.
Zhang, H., Feng, X., Zhu, J., Sapkota, A., Meng, B., Yao, H., et al., 2012. Selenium in soil inhibits mercury uptake and translocation in rice (*Oryza sativa* L.). Environ. Sci. Technol. 46, 10040–10046.
Zhao, F.J., Ma, Y.B., Zhu, Y.G., Tang, Z., McGrath, S.P., 2015. Soil contamination in China: current status and mitigation strategies. Environ. Sci. Technol. 49, 750–759.